A&A 470, 597–603 (2007)
DOI: 10.1051/0004-6361:20066759

Astronomy & Astrophysics

An accurate determination of the distance to the Pipe nebula⋆,⋆⋆

F. O. Alves and G. A. P. Franco

Departamento de Física – ICEx – UFMG, Caixa Postal 702, 30.123-970 Belo Horizonte, Brazil
e-mail: [falves;franco]@fisica.ufmg.br

Received 16 November 2006 / Accepted 27 March 2007

ABSTRACT

Aims. We seek an accurate distance to the Pipe nebula.
Methods. The *B*-band linear polarimetry collected for stars from the *Hipparcos* catalogue is used to investigate the dependence of the measured interstellar polarization as a function of the star's trigonometric parallax.
Results. The linear polarization obtained for 82 *Hipparcos* stars in the general direction of the Pipe nebula are presented and analysed. The distribution of the obtained position angles suggests the existence of two polarizing components. One of them has low average column density and seems to be closer than ∼70 pc to the Sun, while the other component has a higher column density and seems to belong to a very extended interstellar structure. The obtained parallax-polarization diagram indicates a low degree of polarization for stars with $\pi_{\rm H} > 8$ mas, while a steep rise in polarization is observed for stars with $\pi_{\rm H} \approx 7$ mas, corresponding to a distance of approximately 140 pc.
Conclusions. Our analysis suggests a distance of 145 ± 16 pc to de Pipe nebula, meaning that this cloud is part of the Ophiuchus dark cloud complex. There is evidence that the largest filament of the Pipe nebula has collapsed along the magnetic field lines, indicating that magnetic pressure plays an important role in the evolution of this cloud.

Key words. ISM: clouds – ISM: individual objects: Pipe nebula – stars: distances – stars: individual objects: Hipparcos – techniques: polarimetric

1. Introduction

The knowledge of accurate distances to molecular clouds is crucial for calibrating the physical parameters associated with them. Elegant methods for analysing star counts have been worked out by many astronomers and are frequently used to estimate distance, extinction power, and radial extension of interstellar clouds. However, these techniques are unable to give accurate distances since they rely on assumptions that may be inadequate for the region under investigation.

Another classical approach has been to use the photometry of dense grids of stars in a photometric system able to measure accurate colour excesses and provide rather precise photometric distances. Strömgren photometry has been successfully applied for this purpose, but stars with spectral types later than G2 – G5 have not been accurately calibrated in this photometric system.

The availability of high-quality *Hipparcos* trigonometric parallaxes has inspired alternative methods. For instance, Knude & Høg (1998) combined the (B−V) provided by the *Hipparcos* and *Tycho* catalogues with spectral classification from the literature to estimate colour excesses, and to further construct colour excess vs. distance diagrams for several local interstellar clouds. In spite of this method being very useful as a first attempt at estimating the distance to local interstellar clouds, the use of spectral types retrieved from survey catalogues may jeopardise the accuracy of the obtained result.

The literature provides many examples where *Hipparcos* parallaxes are combined with other measurements in order to yield distance estimates to objects of interest. For instance, in a previous work we successfully combined *Hipparcos* parallaxes with linear polarimetry using CCD imaging to investigate the distribution of the interstellar medium in the vicinity of the dark cloud Lupus 1 (Alves & Franco 2006).

In this paper we present the results of *B*-band linear polarimetry using CCD imaging obtained for stars selected from the *Hipparcos* catalogue (ESA 1997) with lines of sight toward the Pipe nebula, a dark cloud that seems to be associated with the large Ophiuchus molecular complex.

Although apparently a potential site for stellar formation, the Pipe nebula has not attracted attention until recently. The detailed map of ^{12}CO obtained by Onishi et al. (1999) for the whole Pipe nebula point to a mass of $\sim 10^4\ M_\odot$ and indicates that the nebula consists of many filamentary structures. In spite of the many identified C^{18}O cores whose masses are typically ∼30 $M_\odot$, star formation seems to be active only on Barnard 59 (B 59), located at the northwestern extremity of the nebula. However, there is evidence that B 59 is producing young stars with high efficiency (Brooke et al. 2007). Based upon stars from the 2MASS catalogue, Lombardi et al. (2006) produced a high-resolution extinction map of the Pipe nebula. The near infrared extinction map correlates well with the molecular one and corroborates the estimated mass.

Previous distance estimates suggest that the Pipe nebula is a local cloud; however, the estimated values are rather uncertain. Onishi et al. (1999) suggest a distance of ∼160 pc, supposing that this cloud is connected with the Ophiuchus dark cloud complex (they assumed the value estimated by Chini 1981). Lombardi et al. (2006) obtained 130^{+13}_{-20} pc from a method similar to the one applied by Knude & Høg (1998), in agreement with the value suggested by de Geus et al. (1989) and Bertout et al. (1999)

⋆ Based on observations collected at Observatório do Pico dos Dias, operated by Laboratório Nacional de Astrofísica (LNA/MCT, Brazil).
⋆⋆ Tables 1 and 2 are only available in electronic form at http://www.aanda.org

for the distance to the Ophiuchus complex (note that de Geus et al. formally estimate a distance range of 60−205 pc for the Ophiuchus dark clouds, with their centre defined as 125 ± 25 pc).

The good quality of our polarimetric data allows us to probe the interstellar medium in the direction of the Pipe nebula and to obtain an accurate distance to this cloud.

2. Observations and data reduction

The polarimetric data were collected with the IAG 60 cm telescope at the Observatório do Pico dos Dias (LNA/MCT, Brazil) in missions conducted from 2003 to 2005. These data were obtained with the use of a specially adapted CCD camera to allow polarimetric measurements – for a suitable description of the polarimeter see Magalhães et al. (1996). The *B*-band linear polarimetry using CCD imaging was obtained for 82 *Hipparcos* stars with trigonometric parallaxes $\pi_{\rm H} \geq 5$ mas, which corresponds to a distance coverage up to 200 pc and ratios of the observational error to the trigonometric parallax given by $\sigma_{\pi_{\rm H}}/\pi_{\rm H} \leq 1/5$. The selected stars have lines of sight toward a large region around the Pipe nebula, limited by Galactic coordinates: $-5^\circ < l < +4^\circ$, $+1^\circ < b < +9^\circ$, covering an area slightly larger than the one surveyed in molecular lines by Onishi et al. (1999).

When in linear polarization mode, the polarimeter incorporates a rotatable, achromatic half-wave retarder followed by a calcite Savart plate. The half-wave retarder can be rotated in steps of 22.5, and one polarization modulation cycle is covered for every 90° rotation of this waveplate. This arrangement provides two images of each object on the CCD with perpendicular polarizations (the ordinary, $f_{\rm o}$, and the extraordinary, $f_{\rm e}$, beams). Rotating the half-wave plate by 45° yields in a rotation of the polarization direction of 90°. Thus, at the CCD area where $f_{\rm o}$ was first detected, now $f_{\rm e}$ is imaged and vice versa. Combining all four intensities reduces flatfield irregularities. In addition, the simultaneous imaging of the two beams allows observing under non-photometric conditions and, at the same time, the sky polarization is practically canceled. Eight CCD images were taken for each star with the polarizer rotated through 2 modulation cycles of 0°, 22.5, 45°, and 67.5 in rotation angle. For each star, an optimum integration time was chosen to obtain a high signal-to-noise ratio, but they stay below the CCD saturation level.

The CCD images were corrected for readout bias, zero level bias, and relative detector pixel response. After these normal steps of CCD reductions, we performed photometry on the pair of polarized stellar images in each of the eight frames of a given star using the IRAF DAOPHOT package. In many cases, we gathered as much as $\sim 10^6$ counts per stellar beam after performing aperture-photometry. From the obtained file containing count data, we calculate the polarization by using a set of specially developed IRAF tasks (PCCDPACK package; Pereyra 2000). This set includes a special purpose FORTRAN routine that reads the data files and calculates the normalized linear polarization from a least-square solution that yields the per cent linear polarization (P), the polarization position angle (θ, measured from north to east), and the per cent Stokes parameters Q and U, as well as the theoretical (i.e., the photon noise) and measured (σ_P) errors. The last are obtained from the residuals of the observations at each wave-plate position angle (ψ_i) with respect to the expected $\cos 4\psi_i$ curve and are consistent with the photon noise erros (Magalhaes et al. 1984). For a good review of the basic concepts and error analysis for polarimetric data obtained with dual-beam instruments, the reader is referred to Patat & Romaniello (2006).

Zero-polarization standard stars were observed every run to check for any possible instrumental polarization and for systematic errors of our polarimetry. The measured polarizations proved to be small and in good agreement with the values listed by Turnshek et al. (1990). The reference direction of the polarizer was determined by observing polarized standard stars (Turnshek et al. 1990), complemented with polarized stars from the catalogue compiled by Heiles (2000). The present project shared some of the observing nights with the one used to collect the data described in our previous work (Alves & Franco 2006), to which we refer the reader for a detailed description of the standard stars used and their standard errors.

Table 1 displays the obtained results for the observed stars, together with their identification in the *Hipparcos* (HIP) catalogue (Col. 1), the Michigan two-dimensional classification (Houk 1982; Houk & Smith-Moore 1988), when available (Col. 2), equatorial coordinates for the equinox 2000.0 (Cols. 3 and 4), Galactic coordinates (Cols. 5 and 6), visual magnitude (Col. 7), trigonometric parallax and standard error (Cols. 8 and 9), polarization and measured error (Cols. 10 and 11), and the orientation angle of the polarization vector (Col. 12), respectively. The polarization measured errors, σ_P, are smaller than 0.08% for all observed stars. They are even substantially smaller than this in many cases because of the large gathered counts of $\sim 10^6$ and the small systematic errors of our polarimeter. This accuracy is corroborated by the small errors found for the zero polarization standard stars (Alves & Franco 2006, Table 1).

As mentioned earlier, an optimum integration time was chosen to obtain a good signal-to-noise ratio for the selected target. Because the targets were usually bright, most of the obtained CCD frames only allowed accurate polarization measurements for the *Hipparcos* program stars, however, in few cases we were able to get the degree of polarization for other stars appearing in the frames. Since this information will be useful in our later discussion, these results are introduced in Table 2, which gives the star's identification, when available (Col. 1), equatorial coordinates for equinox 2000.0 (Cols. 2 and 3), Galactic coordinates (Cols. 4 and 5), polarization and measured error (Cols. 6 and 7), and the orientation angle of the polarization vector (Col. 8), respectively.

3. The sightline toward the Pipe nebula

3.1. Magnetic field structure

Based upon data from the 2MASS catalogue, Lombardi et al. (2006) constructed a high-resolution extinction map of the Pipe nebula. The area covered by the map basically coincides with the one investigated here. In Fig. 1 we overlay the obtained polarization vectors in this extinction map. Since most of the observed stars show a low degree of polarization and these value are not essential at this stage of our analysis, we have plotted polarized vectors proportional to the square root of the polarization degree: with this convention one gets a better view of the orientation pattern. We interpret the polarization of background stars as due to dichroic absorption by a medium of magnetically aligned grains. The polarization position angles therefore map the global structure of the magnetic field within the medium.

At first glance we note, as indicated by the few highly polarized stars in Fig. 1, that the largest filament from $(l, b) \approx (0^\circ, 4^\circ)$ to $(l, b) \approx (357^\circ, 7^\circ)$, corresponding to the "stem" of the "pipe", is roughly perpendicular to the large-scale magnetic field shown by the polarized stars ($P \gtrsim 1\%$) in the region. This orientation suggests that the cloud collapse was steered preferentially along

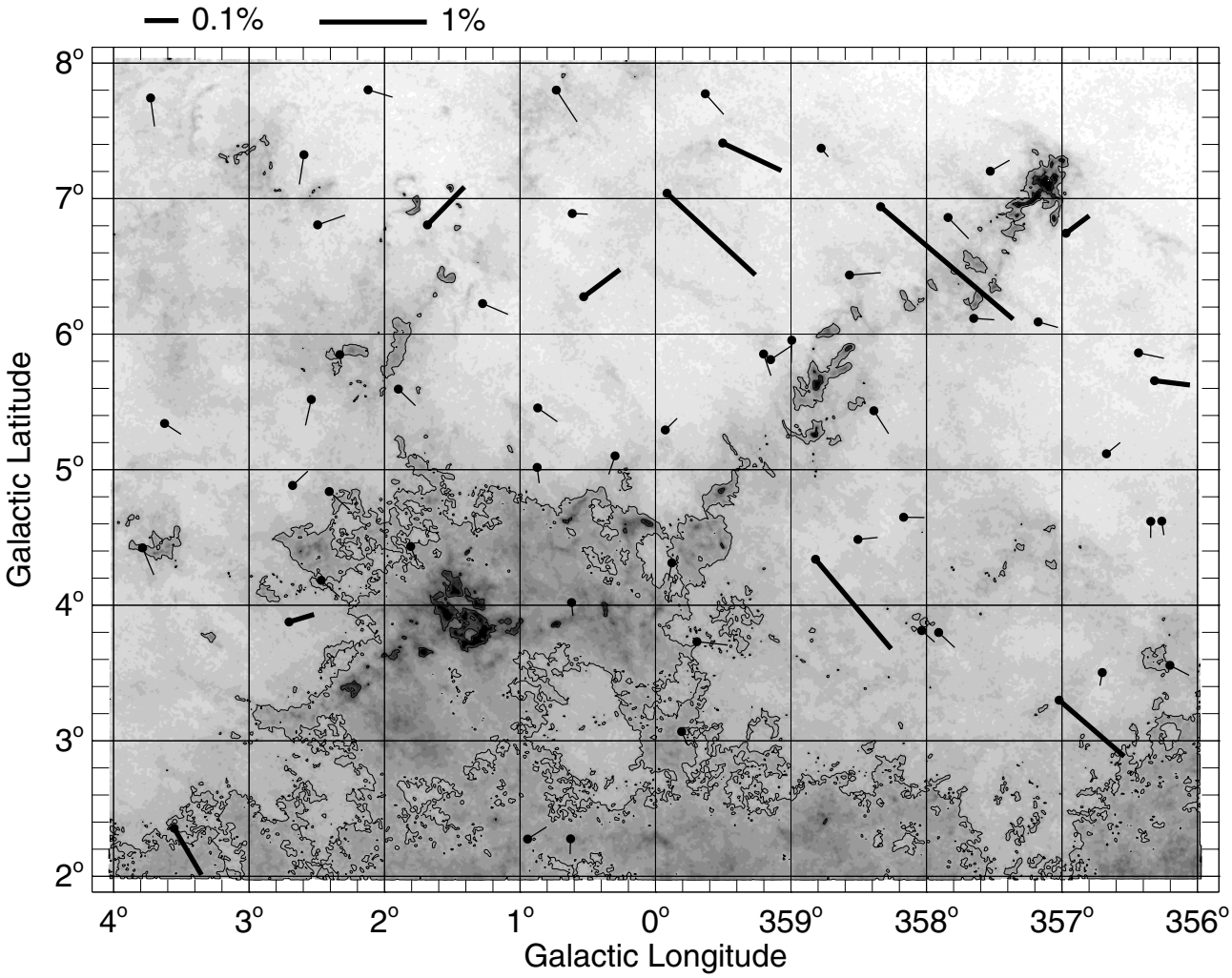

Fig. 1. Dust extinction map of the Pipe nebula molecular complex obtained by Lombardi et al. (2006), contour levels in steps of $0\overset{m}{.}5$ and lowest contour $A_K = 0\overset{m}{.}5$. The positions of the observed *Hipparcos* stars are marked by the filled circles, and the lines give the obtained polarization vectors. The lengths of these vectors are proportional to the square root of the degree of polarization, according to the scale indicated in the upper left-hand corner. Thick lines refer to measurements having $P/\sigma_P \geq 4$.

the field lines and that magnetic pressure continues to support the cloud in the direction of the elongation. In the stellar formation scenario proposed by Shu et al. (1987), this situation should culminate in the formation of low-mass stars, similar to what is observed at other star formation sites, such as the Chamaeleon I, Lupus, and Taurus-Auriga dark clouds (McGregor et al. 1994; Strom et al. 1988; Tamura & Sato 1989, and references therein).

A more accurate analysis of Fig. 1 shows, however, some stars having polarization almost orthogonal to the one presented by stars with a higher degree of polarization. This fact led us to suppose the existence of two absorbing components subject to almost orthogonal magnetic fields. This supposition may be tested by analysing the distribution of the obtained position angles. However, the uncertainty in this quantity correlates with the signal-to-noise of the polarization measurement, which is P/σ_p (see for instance, Naghizadeh-Khouei & Clarke 1993), and since the majority of the observed stars show a low degree of polarization, the signal-to-noise is usually small for our objects. To avoid polluting the distribution of the polarization angles by large uncertainties, only stars having $P/\sigma_P \geq 2.0$ were considered. The obtained distribution is given in Fig. 2 (*left-hand panel*) and seems to support the existence of two, almost orthogonal, components. The shaded area in this histogram represents stars having $P/\sigma_P \geq 4.0$. Note that the bin [0°, 30°] was shifted by 180° and appears at the end of the histogram. Stars belonging to the first component (~60°) show a low degree of polarization, suggesting an origin in a low column-density medium (hereafter "diffuse component"), while many stars in the second component (~160°) are more heavily polarized (hereafter "dense component"). We note that no stars introduced in Table 2 were included in the histogram in Fig. 2; however, all star showing a relatively high degree of polarization, in that table, have a position angle in the interval defined by the dense component.

One should be aware that a larger and more accurate sample is required in order to establish the existence and characteristics of these two components; however, previous works have already pointed out the complex nature of the magnetic field toward this direction in the solar neighbourhood. The skyplots presented by Axon & Ellis (1976, Figs. 1a and b) show this complexity around the area investigated here and support the existence of two dominant components. More recently, Leroy (1999) analysed polarization data for stars with *Hipparcos* parallaxes in the solar vicinity. The results indicate the existence, in some directions, of patches of polarizing material closer than 70 pc. That seems to be the case of the diffuse component presented by our stellar sample. Figure 2 (*right-hand panel*) shows the distribution

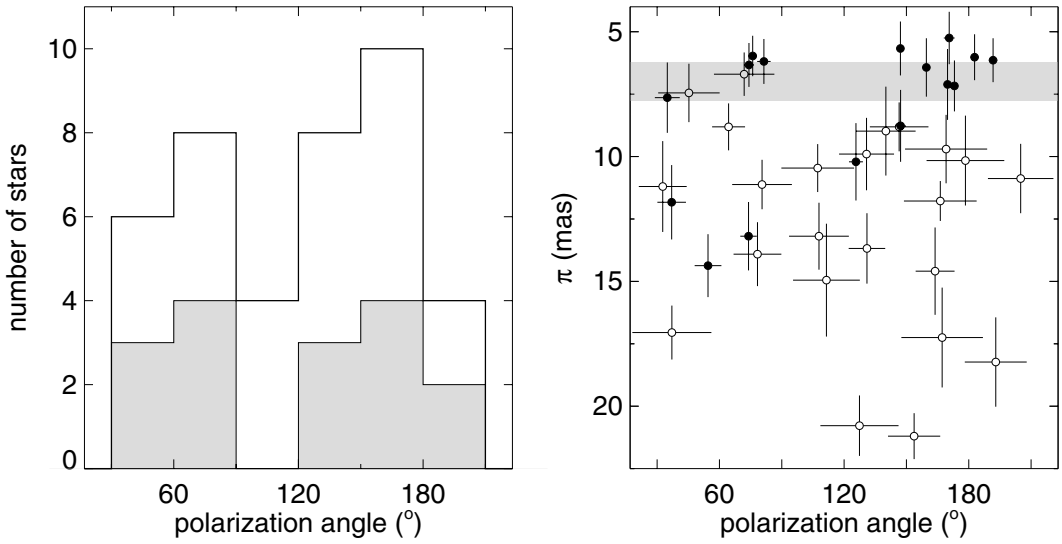

Fig. 2. *left*: distribution of the observed position angles. The figure shows the histogram obtained for 40 stars having $P/\sigma_P \geq 2$. The shaded area represents stars with $P/\sigma_P \geq 4$. The distribution clearly suggests the existence of two components. *right*: distribution of position angles as a function of the *Hipparcos* parallaxes, where stars with $P/\sigma_P \geq 4$ are represented by filled circles. The $\pm 1\sigma_\theta$ were estimated using the method proposed by Naghizadeh-Khouei & Clarke (1993). The shaded area indicates the suggested distance interval (145 ± 16 pc) to the Pipe nebula (see text).

of polarization angles as a function of the *Hipparcos* parallaxes. If one take into account those stars belonging to the group with higher signal-to-noise, ($P/\sigma_P \geq 4$), the diffuse component seems to appear at a distance of about 70 pc ($\pi_{\rm H} = 14.37$ mas – HIP 86226). The dense component seems to set in farther than that.

It is remarkable, from Fig. 1, that the two stars having lines-of-sight on each side of the northwestern extremity of the Pipe nebula (close to the location of B 59) show position angles that are almost aligned with the direction of the stem and supposedly associated to the diffuse component. Our measured polarization for HIP 84144 (left-hand side of the nebula) has a low signal-to-noise and consequently a very suspicious value for the position angle; however, HIP 84175 (right-hand side of the nebula) has a high signal-to-noise and its position angle can be trusted. This is among the three stars having $P/\sigma_P \geq 4$, position angle $\theta \sim 75°$, and a distance compatible with the one expected for the Pipe nebula (see Fig. 2 (*right-hand panel*) and the discussion introduced in Sect. 4), the other two stars are clearly identifiable to the left of HIP 84144 in Fig. 1.

In a forthcoming observational program we are planning to acquire deep CCD imaging polarimetry for lines of sight through dense cores in the Pipe nebula. The purpose of the intended data is to investigate the geometry and influence of the magnetic field over this nebula in detail. It is particularly interesting to examine the geometry of the magnetic field in the vicinity of B 59.

3.2. Interstellar dust distribution

Figure 3 shows a plot of the linear polarization against stellar parallax. The obtained distribution clearly shows a small degree of polarization at large parallaxes, for $\pi_{\rm H} > 8$ mas, followed by a remarkably steep rise in polarization that occurs close to $\pi_{\rm H} \approx 7$ mas, indicating that the Pipe nebula is located at a distance of ∼140 pc. This value is consistent with the distance suggested by Lombardi et al. (2006). Before trying to better estimate the distance to the Pipe nebula, it is instructive to compare our parallax-polarization diagram with the parallax-extinction

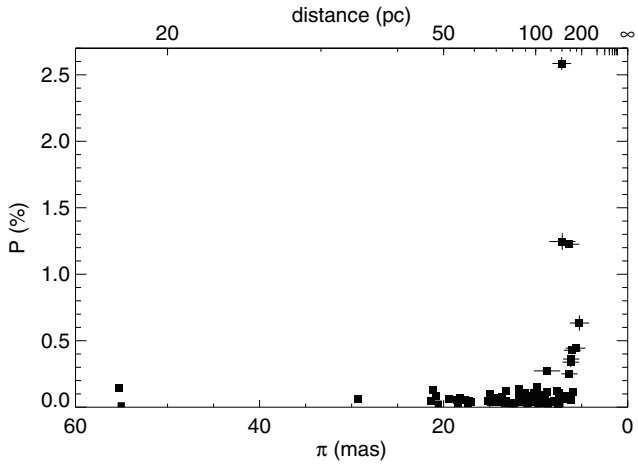

Fig. 3. The obtained parallax-polarization diagram. Error bars ($\pm 1\sigma_\pi$, $\pm 1\sigma_P$) are indicated for stars with degree of polarization higher than 0.25%.

diagram obtained by Lombardi et al. (2006, Fig. 11). As pointed out by those authors, their diagram shows large scatters in the parallax and estimated interstellar absorption making the interpretation not straightforward. It is worthwhile noting that the large scatters in parallax are mainly caused by their being less restrictive in the selection criteria then we were; i.e. they accepted all stars with ratio of the observational error to the trigonometric parallax given by $\sigma_{\pi_{\rm H}}/\pi_{\rm H} < 1$, while we used $\sigma_{\pi_{\rm H}}/\pi_{\rm H} \leq 1/5$. On the other hand, uncertainties in spectral classification cause scattering in the estimated extinction values. Because of that, the distance where the reddening sets in cannot be clearly defined in their diagram as it can be in ours.

The parallax-polarization diagram shown in Fig. 3 suggests that the volume located in front of the Pipe nebula is almost free of interstellar dust. The similarity of this diagram to the one obtained for a region ∼23° apart in the Lupus dark cloud complex is remarkable (Alves & Franco 2006, see Fig. 4a). Both diagrams indicate that the clouds composing the Ophiuchus and

Lupus complexes may somehow be physically associated. It immediately raises the question of how these clouds are related to the structure of the Galactic environment in the solar neighbourhood. Current evidence suggests that the solar system is embedded in an irregularly-shaped low-density volume ("local cavity") of the local interstellar medium, partially filled with hot ($\sim 10^6$ K) coronal gas ("Local Bubble", or LB for short) detectable in soft X-rays (e.g. Snowden et al. 1998; Sfeir et al. 1999; Vergely et al. 2001; Lallement et al. 2003, and references therein). Although there is some agreement that the hot component has likely been produced by a series of several supernovae explosions within the past few million years (e.g. Maíz-Apellániz 2001; Berghöfer & Breitschwerdt 2002; Fuchs et al. 2006, and references therein), the global characteristics of all the interstellar medium in the solar neighbourhood is a debated issue.

Two scenarios have been suggested for explaining at least some of the main observational facts. One scenario claims the interaction of two physically separate phenomena. The LB is interacting with its neighbouring superbubble shell (Loop I) generated by stellar winds or supernovae from the nearby Scopius-Centaurus OB association, in turn resulting in a circular ring of neutral hydrogen at the location of the interaction of these two shells. Inside this ring there is a sheet of neutral hydrogen, forming a "wall" that separates the two bubbles (Egger & Aschenbach 1995). The other scenario argues that the LB is part of an asymmetrically-shaped superbubble created by stellar wind and supernovae explosions associated with the Sco-Cen association. The LB was sculpted by the free expansion of this superbubble into the low-density interarm region surrounding the solar system (Frisch 1981, 1995).

In the interacting bubbles' model, the wall has an estimated neutral hydrogen column density, $N(\mathrm{H\,I})$, of $\sim 10^{20}$ cm^{-2} (Egger & Aschenbach 1995; Sfeir et al. 1999), which corresponds to $E(b-y) \approx 0\overset{\mathrm{m}}{.}013$ (adopting the gas-to-dust ratio $N(\mathrm{H})/E(b-y) = 7.5 \times 10^{21}$ atoms cm^{-2} mag^{-1} suggested by Knude 1978), and to a maximum expected degree of polarization of $\approx$0.16% (Serkowski et al. 1975). It is worth noting that the linear polarization is by definition a positive quantity, suffering a positive bias that is not negligible at low polarization levels. By applying the method introduced by Simmons & Stewart (1985), one may estimate the unbiased degree of polarization and confidence intervals. Most of the stars introduced in Table 1 showing low degree of polarization may in fact be totally unpolarized, confirming the low-column density nature of the observed volume. Our sample shows, however, 6 stars within 100 pc from the Sun which seem to present some degree of polarization, supposedly caused by the diffuse component mentioned earlier in Sect. 3.1. One of these stars is HIP 83578 ($d = 76^{+9}_{-7}$ pc) with a corrected degree of polarization $P = 0.118\%$ ($P = [0.076, 0.160]\%$ – confidence interval at 99%, Simmons & Stewart 1985), which suggests the existence of absorbing material at distances smaller than $\sim$70 pc with a density consistent with the expected one for the interface wall between the Local and Loop I bubbles. Although similar results are obtained for the remaining 5 stars, they do not prove the existence of an interface separating our local cavity from the Loop I bubble. Indead, the obtained polarization may be produced by the interstellar matter outflowing from the Loop I bubble, in the sense proposed by Frisch (1995).

Moreover, in a previous polarimetric investigation Tinbergen (1982) identified a dust cloud at a distance between 0 and 20 pc from the Sun, with an inferred gas column density of $\sim 10^{19}$ atoms cm^{-2} and a very patchy distribution, since only about 30% of the stars in the surveyed region ($350° < l < 20°$, $-40° < b < -5°$) showed polarization above 2σ. High-resolution interstellar line studies also show a complex multicomponent structure of the interstellar medium in this Galactic direction (e.g., Crawford 1991; Génova et al. 1997).

4. Distance

Our stellar sample contains 19 stars with trigonometric parallaxes within the range $6 \leq \pi_{\mathrm{H}} \leq 8$, corresponding to the distance interval $125 \leq d_\pi \leq 167$ pc. Among them, 10 show a low degree of polarization, i.e. measured polarization smaller than 0.1%, indicating that they are supposedly foreground objects and may be used to impose a minimum value for the distance to the Pipe nebula. The farthest of them, HIP 84930, has a corrected degree of polarization $P = 0.044\%$ ($P = [0.000, 0.128]\%$) and measured parallax of $\pi_{\mathrm{H}} = 6.12 \pm 1.01$ mas, which locates this star at 163^{+33}_{-23} pc. Based on the data of this star alone, the lower limit for the value of the distance to the Pipe nebula would be 140 pc, which corresponds to the upper limit suggested by Lombardi et al. (2006). At only $\sim 4'$ from HIP 84930 we find HIP 84931, another object with a low degree of polarization and a measured parallax of $\pi_{\mathrm{H}} = 6.70 \pm 0.87$ mas (149^{+23}_{-17} pc).

Figure 4 shows images from the Digitized Sky Survey centred, respectively, on HIP 83194 *(left-hand panel)* and HIP 84144 *(right-hand panel)*, two frames from which we were able to measure polarization for some of the field stars (see Table 2). Owing to the measured low degree of polarization ($P = [0.000, 0.041]\%$ for HIP 83194 and $P = [0.000, 0.156]\%$ for HIP 84144, confidence interval at 99%), both stars seem to be foreground objects at $\pi_{\mathrm{H}} = 7.37 \pm 1.14$ mas (136^{+25}_{-19} pc) and $\pi_{\mathrm{H}} = 7.04 \pm 0.95$ mas (142^{+22}_{-17} pc), respectively, while the field stars prove the existence of polarizing material beyond the location of HIP 83194 and HIP 84144 – none of the field stars have accurate distance determination. HIP 83194 lies outside the limits of Fig. 1; and HIP 84144, as mentioned in Sect. 3.1, is the star on the left-hand side of the northwestern extremity of the Pipe nebula having a polarization position angle supposedly aligned with the Pipe nebula's stem. The field stars show polarization with position angles consistent with the one presented by stars affected by the dense component, and interestingly, the two stars in the field of HIP 84144 show polarization roughly perpendicular to the large axis of the Pipe nebula.

The upper limit for the distance to the Pipe nebula is imposed by the star with the highest degree of polarization in our sample, i.e. HIP 84391. Its measured parallax of $\pi_{\mathrm{H}} = 7.17 \pm 1.02$ mas (140^{+23}_{-18} pc) limits the distance to $\sim$160 pc. Two other stars show a degree of polarization higher than 1%, HIP 84695 at $\pi_{\mathrm{H}} = 7.11 \pm 1.42$ mas (141^{+35}_{-24} pc), and HIP 85318 at $\pi_{\mathrm{H}} = 6.43 \pm 1.17$ mas (156^{+34}_{-25} pc). A weighted average of these three parallaxes yields $\langle\pi\rangle = 6.91 \pm 0.68$ mas (145^{+16}_{-14} pc), which can be accepted as the best estimate of the distance to the Pipe nebula. This value is about 10% larger than the one recently suggested by Lombardi et al. (2006).

Three stars deserve a comment. They are the objects having $P/\sigma_p \geq 4$ and position angle $\theta \sim 75°$, which were mentioned in Sect. 3.1. Their estimated distance locate them somewhere between the front and the back sides of the Pipe nebula, and they show a degree of polarization that is intermediate between the unpolarized foreground stars and the rather polarized background ones. We designated them "midground" objects in Table 3, which summarises the important parameters of the stars relevant to the estimate of the distance to the Pipe nebula. An interesting question that needs further investigation concerns the origin of the polarization shown by these stars: is it produced

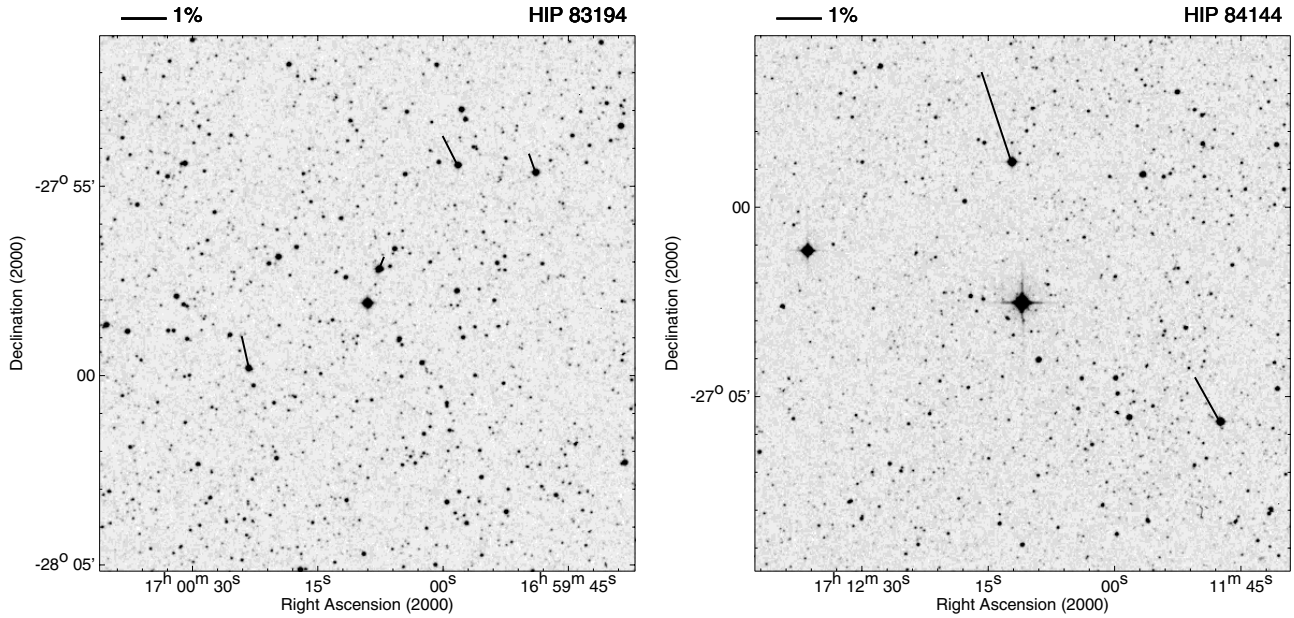

Fig. 4. Measured polarization for stars in the vicinity of HIP 83194 (*left-hand panel*) and HIP 84144 (*right-hand panel*). The *Hipparcos* stars are centred on each panel. The length of the vectors correlates linearly with the degree of polarization, according to the scale indicated in the left-hand corner.

Table 3. Stars relevant to the estimate of the distance to the Pipe nebula.

HIP	l (°)	b (°)	$P_{\rm min}/P_{\rm max}$ [a] (%)	$d_{\rm min}/d_{\rm max}$ [b] (pc)	$A_{\rm K}$ [c] (mag)
foreground objects					
83194	355.2	+8.8	0.000/0.041	117/161	–
84144	357.6	+7.2	0.000/0.156	125/164	0.12
84930	359.2	+5.9	0.000/0.128	140/196	0.16
84931	359.1	+5.8	0.000/0.163	132/172	0.16
midground objects					
84175	357.0	+6.7	0.089/0.135	147/194	0.08
85071	0.5	+6.3	0.191/0.307	138/184	0.15
85154	1.7	+6.8	0.235/0.438	141/189	0.23
background objects					
84391	358.3	+6.9	2.360/2.762	122/163	0.10
84695	359.9	+7.0	1.045/1.426	117/176	0.19
85318	358.8	+4.3	1.110/1.319	131/190	0.24

[a] Lower/upper value for the degree of polarization at 99% confidence level (Simmons & Stewart 1985); [b] estimated $1\sigma_\pi$ minimum/maximum trigonometric distance; [c] estimated from the dust extinction map constructed by Lombardi et al. (2006).

by a foreground low column density medium or is the magnetic field in the vicinities of the Pipe nebula characterised by two orthogonal components?

The last column of Table 3 gives the dust extinction, $A_{\rm K}$, estimated from the extinction map obtained by Lombardi et al. (2006), and shows that all stars, but HIP 83194 located outside the area mapped by them, have line-of-sight toward directions affected by dust extinction. In fact, HIP 84391, the star showing the highest degree of polarization in our sample, seems to be in the direction of the second lowest dust extinction among them, which is proof that the unpolarized stars listed in this table are really foreground objects.

It is interesting to compare the obtained distance to the Pipe nebula with estimates for sites of star formation in its neighbourings. Unlike the Pipe nebula that has attracted attention only recently, many objects in its surroundings have been the subject of numerous investigations. One of the most studied objects is the ρ Ophiuchi cloud complex, one of the nearest star-forming regions, located about 14° to the northwest of the Pipe nebula, on the edge of the Upper Scorpius subgroup in the Sco-Cen OB association. Quoted distances to the Ophiuchus dark clouds comprise 125 ± 25 pc (de Geus et al. 1989), 128 ± 12 pc (Bertout et al. 1999), and 165 ± 20 pc (Chini 1981). Recently Vaughan et al. (2006) analysed the X-ray halo around GRB 050724, which has a line of sight through the Ophiuchus molecular complex, concluding that the observed narrow halo must have been caused by a concentration of dust at a distance of 139 ± 9 pc from the Sun. The latter seems to be the best estimated value so far for the distance to the Ophiuchus dark cloud complex and is in excellent agreement with the distance we obtained for the Pipe nebula. It is worthwhile noting that the distance we obtained for the Pipe nebula is also in perfect agreement with the distance of 145 ± 2 pc suggested for the Upper Scorpius subgroup (de Bruijne et al. 1997; de Zeeuw et al. 1999).

Moreover, the distance obtained for the Pipe nebula is also very similar to the one suggested for the Lupus 1 dark cloud (Franco 2002; Alves & Franco 2006), indicating that the interstellar medium toward these directions may somehow be associated, forming a large interstellar structure. It must be noted that our polarization data do not support the scenario proposed by Welsh & Lallement (2005), which depicts the distribution of the interstellar gas toward the Ophiuchus and Lupus dark clouds. According to their picture, dense gas exists at a distance of ∼50 pc from the Sun toward these directions, which is not confirmed by our polarization data, unless the gas is disassociated from dust.

5. Conclusions

By analysing the obtained B-band CCD imaging linear polarimetry for 82 *Hipparcos* stars with the line of sight toward the area containing the Pipe nebula, we have reached the following conclusions:

– There is evidence that the polarization angles have an almost orthogonal two-component distribution. One of these

components, if it exists, could be caused by a low column-density medium ($\sim 10^{20}$ atoms cm^{-2}) closer than $\sim$70 pc, which may be either related to the interface wall between the Local and Loop I bubbles or to some other kind of interstellar structure. The other component seems to be caused by a higher column-density medium.

– We found that the "stem" of the "pipe" is aligned perpendicularly to the general direction of the local magnetic field provided by the dense component. This fact may be an indication that the stem is the result of a magnetically controlled collapse. To test this hypothesis further, we are planning new observations to prove the densest parts of the Pipe nebula's "stem".
– The distribution of linear polarization against trigonometric parallaxes suggests that the Pipe nebula is located at a distance of 145 ± 16 pc from the Sun. The volume in front of this cloud is almost empty of absorbing material. However, few stars up to about 100 pc show clear signs of polarization, which may be caused either by an extended low column density medium or by small diffuse clouds.

As a final remark, we notice that the Pipe nebula seems to provide a particularly suitable laboratory in which to study the physical processes experienced by the interstellar clouds during the phase of contraction to form low-mass stars. Such potential has been proven by the recent identification of more than 150 dense cores in this cloud (Alves et al. 2007). Additionally, in the scenario proposed by Preibisch & Zinnecker (1999, 2007), the Pipe nebula may be the place where the next generation of nearby stars will be formed in a sequence just after the association in ρ Ophiuchi. In fact, this process has already started in the north-western part of the cloud, as shown by the evidence in B 59, where there are at least 5 Hα known emission-line stars and at least 20 other candidate low-mass young stars (Brooke et al. 2007), which suggest that this core is producing young stars with high efficiency.

Acknowledgements. We thank Dr. Marco Lombardi for generously supplying the Pipe nebula extinction map prior publication. This research has made use of the *Hipparcos* catalogue (ESA SP-1200, 1997) and of the Digitized Sky Survey produced at the Space Telescope Science Institute under US Government grant NAG W-2166, which is based on photographic data obtained using the UK Schmidt Telescope and the Palomar Sky Survey. We made extensive use of NASA's Astrophysics Data System (NASA/ADS) and the SIMBAD database, operated at the CDS, Strasbourg, France. We thank the staff of the Observatório do Pico dos Dias (LNA/MCT, Brazil) for their hospitality and invaluable help during our observing runs. We are also grateful to Drs. A. M. Magalhães and A. Pereyra for providing the polarimetric unit and the software used for the reductions of the polarimetric data. We gratefully acknowledge financial support from the Brazilian agencies CNPq and FAPEMIG.

References

Alves, F. O., & Franco, G. A. P. 2006, MNRAS, 366, 238
Alves, J., Lombardi, M., & Lada, C. J. 2007, A&A, 462, L17
Axon, D. J., & Ellis, R. S. 1976, MNRAS, 177, 499
Berghöfer, T. W., & Breitschwerdt, D. 2002, A&A, 390, 299
Bertout, C., Robichon, N., & Arenou, F. 1999, A&A, 352, 574
Brooke, T. Y., Huard, T. L., Bourke, T. L., et al. 2007, ApJ, 655, 364
Chini, R. 1981, A&A, 99, 346
Crawford, I. A. 1991, A&A, 247, 183
de Bruijne, J. H. J., Hoogerwerf, R., Brown, A. G. A., Aguilar, L. A., & de Zeeuw, P. T. 1997, in ESA SP-402: Hipparcos - Venice '97, 575
de Geus, E. J., de Zeeuw, P. T., & Lub, J. 1989, A&A, 216, 44
de Zeeuw, P. T., Hoogerwerf, R., de Bruijne, J. H. J., Brown, A. G. A., & Blaauw, A. 1999, AJ, 117, 354
Egger, R. J., & Aschenbach, B. 1995, A&A, 294, L25
ESA 1997, The Hipparcos and Tycho Catalogues, ESA SP-1200 (Noordwijk: ESA Publications Division)
Franco, G. A. P. 2002, MNRAS, 331, 474
Frisch, P. C. 1981, Nature, 293, 377
Frisch, P. C. 1995, Space Sci. Rev., 72, 499
Fuchs, B., Breitschwerdt, D., de Avillez, M. A., Dettbarn, C., & Flynn, C. 2006, MNRAS, 373, 993
Génova, R., Beckman, J. E., Bowyer, S., & Spicer, T. 1997, ApJ, 484, 761
Heiles, C. 2000, AJ, 119, 923
Houk, N. 1982, in Michigan Spectral Survey, Ann Arbor, Dep. Astron., Univ. Michigan, Vol. 3
Houk, N., & Smith-Moore, M. 1988, in Michigan Spectral Survey, Ann Arbor, Dep. Astron., Univ. Michigan, Vol. 4
Knude, J. 1978, in Astronomical Papers Dedicated to Bengt Stromgren, Copenhagen Univ. Obs., Copenhagen, ed. A. Reiz, & J. Andersen, 273
Knude, J., & Høg, E. 1998, A&A, 338, 897
Lallement, R., Welsh, B. Y., Vergely, J. L., Crifo, F., & Sfeir, D. 2003, A&A, 411, 447
Leroy, J. L. 1999, A&A, 346, 955
Lombardi, M., Alves, J., & Lada, C. J. 2006, A&A, 454, 781
Magalhães, A. M., Rodrigues, C. V., Margoniner, V. E., Pereyra, A., & Heathcote, S. 1996, in Polarimetry of the Interstellar Medium, ASP Conf. Ser., 97, 118
Magalhaes, A. M., Benedetti, E., & Roland, E. H. 1984, PASP, 96, 383
Maíz-Apellániz, J. 2001, ApJ, 560, L83
McGregor, P. J., Harrison, T. E., Hough, J. H., & Bailey, J. A. 1994, MNRAS, 267, 755
Naghizadeh-Khouei, J., & Clarke, D. 1993, A&A, 274, 968
Onishi, T., Kawamura, A., Abe, R., et al. 1999, PASJ, 51, 871
Patat, F., & Romaniello, M. 2006, PASP, 118, 146
Pereyra, A. 2000, Ph.D. Thesis, Univ. São Paulo (Brazil)
Preibisch, T., & Zinnecker, H. 1999, AJ, 117, 2381
Preibisch, T., & Zinnecker, H. 2007, in Triggered Star Formation in a Turbulent ISM, IAU Symp., 237, 270
Serkowski, K., Mathewson, D. L., & Ford, V. L. 1975, ApJ, 196, 261
Sfeir, D., Lallement, R. Crifo, F., & Welsh, B. Y. 1999, A&A, 346, 785
Shu, F. H., Adams, F. C., & Lizano, S. 1987, ARA&A, 25, 23
Simmons, J. F. L., & Stewart, B. G. 1985, A&A, 142, 100
Snowden, S., Egger, R., Finkbeiner, D. P., Freyberg, M. J., & Plueinsky, P. P. 1998, ApJ, 493, 715
Strom, S. E., Strom, K. M., & Edwards, S. 1988, in Galactic and Extragalactic Star Formation, NATO ASIC Proc., 232, 53
Tamura, M., & Sato, S. 1989, AJ, 98, 1368
Tinbergen, J. 1982, A&A, 105, 53
Turnshek, D. A., Bohlin, R. C., Williamson, R. L., et al. 1990, AJ, 99, 1243
Vaughan, S., Willingale, R., Romano, P., et al. 2006, ApJ, 639, 323
Vergely, J.-L., Freire Ferrero, R., Siebert, A., & Valette, B. 2001, A&A, 366, 1016
Welsh, B. Y., & Lallement, R. 2005, A&A, 436, 615

Online Material

Table 1. *B*-band linear polarization of *Hipparcos* stars. For an explanation of each column, see note below.

HIP	Spectral Type	α_{2000} (h m s)	δ_{2000} (° ′ ″)	l (°)	b (°)	V (mag)	$\pi_{\rm H}$ (mas)	σ_π (mas)	P (%)	σ_P (%)	θ (°)
83194	F2 V	17 00 09.08	–27 58 05.7	355.16	8.80	8.45	7.37	1.14	0.005	0.018	177.2
83239	G1/2 V	17 00 40.42	–27 47 32.4	355.37	8.82	8.18	21.37	1.16	0.047	0.025	157.0
83541	K1 V	17 04 27.79	–28 34 55.3	355.24	7.67	6.59	55.31	0.89	0.148	0.056	110.3
83578	G3 V	17 04 52.76	–27 22 59.2	356.27	8.31	8.90	13.19	1.37	0.119	0.016	74.0
83659	B9.5 V	17 05 56.67	–28 52 21.5	355.20	7.24	7.55	6.02	0.92	0.428	0.031	2.8
84076	F3 IV/V	17 11 20.94	–25 01 53.4	359.05	8.52	8.30	9.90	1.45	0.154	0.058	130.8
84131	G0 V	17 11 56.68	–29 28 27.8	355.49	5.83	9.29	11.12	1.57	0.045	0.043	4.1
84144	G8 III	17 12 10.97	–27 02 31.7	357.51	7.20	6.75	7.04	0.95	0.062	0.040	69.6
84147	A0 V	17 12 13.62	–25 15 18.1	358.98	8.23	6.52	8.81	0.94	0.118	0.030	64.4
84175	B9 V(n)	17 12 25.07	–27 45 43.2	356.95	6.74	6.12	5.97	0.81	0.113	0.008	76.0
84181	G2 V	17 12 31.27	–25 13 37.3	359.04	8.19	8.29	11.60	1.33	0.042	0.075	40.4
84284	G0 V	17 13 45.99	–24 03 07.9	0.18	8.63	9.01	11.83	1.49	0.139	0.032	37.0
84314	F2/3 V	17 14 14.25	–26 59 03.3	357.82	6.86	6.64	11.78	0.80	0.076	0.034	166.3
84322	K2 V	17 14 17.77	–28 42 24.4	356.41	5.86	9.34	29.35	1.49	0.063	0.036	29.0
84355	F7 V	17 14 45.32	–28 55 17.2	356.30	5.65	9.28	7.64	1.41	0.124	0.026	34.9
84356	F8/G0 V	17 14 45.74	–25 55 26.0	358.76	7.38	9.12	7.55	1.27	0.011	0.020	161.3
84391	G8 III/IV	17 15 13.23	–26 31 50.2	358.32	6.94	7.63	7.17	1.02	2.585	0.049	173.1
84407	G8 IV	17 15 22.21	–27 58 13.1	357.16	6.09	8.54	10.18	1.11	0.038	0.029	24.2
84416	G0	17 15 28.03	–24 59 33.4	359.62	7.78	9.95	14.59	1.75	0.067	0.020	163.8
84445	B9/9.5 V	17 15 51.36	–30 12 38.2	355.38	4.71	6.20	8.81	0.98	0.038	0.015	146.5
84494	K1 III	17 16 27.67	–25 18 19.5	359.50	7.42	7.14	6.14	0.88	0.354	0.028	55.2
84497	G1 V	17 16 29.87	–27 33 54.9	357.63	6.12	8.22	17.05	1.08	0.042	0.020	37.1
84533	F0 V	17 16 54.32	–30 21 05.0	355.39	4.44	7.27	15.15	1.10	0.045	0.027	8.7
84605	B9.5 V	17 17 39.53	–26 37 44.3	358.55	6.44	6.81	7.45	1.17	0.103	0.042	45.3
84609	G0 V	17 17 41.94	–28 56 17.9	356.65	5.11	8.69	15.19	1.28	0.044	0.034	77.6
84611	G2/3 V	17 17 43.17	–30 46 13.7	355.15	4.06	8.96	13.68	1.41	0.076	0.021	131.0
84636	G3 V	17 18 07.07	–24 04 22.2	0.73	7.81	6.59	21.20	0.92	0.130	0.047	153.7
84665	G3 V	17 18 30.88	–29 33 19.8	356.25	4.61	8.74	10.96	1.35	0.024	0.017	125.1
84684	K0 V	17 18 43.91	–29 29 23.5	356.33	4.61	9.67	17.40	1.80	0.035	0.026	117.0
84695	F2 V	17 18 50.47	–25 10 37.0	359.91	7.05	9.62	7.11	1.42	1.246	0.063	169.8
84761	F6 V	17 19 30.88	–22 59 30.9	1.82	8.15	9.34	9.39	1.68	0.082	0.043	89.2
84806	F5 V	17 20 00.41	–30 25 44.9	355.71	3.85	8.80	9.75	1.29	0.003	0.011	53.4
84851	G8 III/IV	17 20 30.72	–26 32 59.1	358.98	5.96	7.09	7.47	0.91	0.064	0.038	117.2
84888	F7/8 IV + F/G	17 20 54.67	–27 20 39.7	358.38	5.44	7.94	10.21	1.58	0.069	0.039	151.5
84907	K0/1 V + (G)	17 21 07.58	–24 41 00.7	0.61	6.90	8.61	20.58	1.18	0.023	0.045	36.9
84930	A1 IV/V	17 21 24.68	–26 26 05.7	359.19	5.86	8.02	6.12	1.01	0.054	0.031	136.7
84931	A2 V	17 21 25.98	–26 30 04.3	359.14	5.82	7.53	6.70	0.87	0.082	0.033	71.9
84936	G1 V	17 21 31.61	–22 55 33.1	2.14	7.80	8.70	17.63	1.64	0.057	0.060	20.5
84987	G2 V	17 22 13.52	–31 39 28.3	354.97	2.76	9.03	10.88	1.39	0.033	0.014	25.0
84995	F0 V	17 22 22.22	–31 17 50.5	355.29	2.94	8.28	7.07	1.25	0.077	0.049	153.3
84999	G0 V	17 22 24.53	–30 12 14.2	356.19	3.55	8.02	14.81	1.48	0.040	0.029	8.8
85071	A2/3 IV	17 23 09.70	–25 05 51.1	0.53	6.28	7.28	6.33	0.88	0.251	0.021	74.2
85081	G8/K0 V	17 23 17.67	–27 58 01.0	358.16	4.65	9.42	14.78	1.79	0.044	0.029	39.9
85100	F0 V	17 23 32.66	–31 42 01.2	355.10	2.51	7.76	12.34	1.08	0.033	0.021	64.7
85132	K0 IV/V	17 23 53.99	–29 49 15.8	356.69	3.50	7.59	12.56	1.13	0.025	0.021	108.3
85154	K0 III	17 24 03.51	–23 50 39.5	1.69	6.81	6.67	6.19	0.90	0.339	0.038	81.4
85176	F5/6 V	17 24 23.86	–22 48 03.1	2.61	7.32	8.65	14.95	2.26	0.101	0.043	111.5
85215	G0	17 24 45.77	–27 46 42.7	358.50	4.49	9.73	10.08	1.94	0.042	0.024	46.6
85246	G	17 25 10.78	–24 30 20.1	1.28	6.23	9.80	18.23	1.79	0.066	0.027	13.0
85257	F8 V	17 25 17.80	–26 08 45.8	359.92	5.30	9.11	8.10	1.49	0.036	0.038	80.4
85278	A2/3 IV	17 25 29.64	–29 40 14.2	357.01	3.30	6.82	5.25	1.05	0.633	0.057	170.6
85285	G3/5 V	17 25 36.62	–21 37 54.1	3.75	7.73	8.37	20.78	1.21	0.083	0.039	127.4
85299	G3/6 V	17 25 51.17	–28 39 19.0	357.90	3.80	9.03	14.24	1.52	0.042	0.045	167.8
85315	F5 V	17 26 01.34	–23 10 17.4	2.51	6.81	8.19	9.28	1.11	0.090	0.054	57.6
85318	B9/9.5 V	17 26 05.87	–27 35 58.3	358.81	4.34	7.49	6.43	1.17	1.226	0.027	159.6
85320	G8 IV/V	17 26 06.87	–28 32 35.9	358.03	3.81	7.78	8.71	1.14	0.026	0.029	169.6
85391	B9.5/A0 V	17 26 55.30	–25 56 36.2	0.30	5.11	6.42	7.71	0.85	0.049	0.067	102.0
85395	G3 V	17 27 00.86	–25 16 17.5	0.87	5.46	9.49	7.99	1.35	0.049	0.050	178.2
85521	F3 IV/V	17 28 38.76	–25 30 38.1	0.87	5.02	7.06	9.06	1.81	0.028	0.040	125.0
85524	F0 V	17 28 40.84	–31 23 03.0	355.97	1.77	7.60	11.12	0.99	0.110	0.044	80.5
85538	G1/2 V	17 28 49.94	–26 43 46.5	359.87	4.32	8.63	13.19	1.34	0.043	0.017	107.9
85548	G2 V	17 29 00.20	–24 20 11.1	1.90	5.60	8.39	17.25	2.00	0.049	0.024	167.2

Table 1. continued.

HIP	Spectral Type	α_{2000} (h m s)	δ_{2000} (° ′ ″)	l (°)	b (°)	V (mag)	$\pi_{\rm H}$ (mas)	σ_π (mas)	P (%)	σ_P (%)	θ (°)
85561	K5 V	17 29 06.74	–23 50 09.4	2.34	5.85	9.61	55.03	1.68	0.010	0.041	126.8
85681	F5 V	17 30 33.65	–27 12 11.8	359.69	3.73	8.55	11.20	1.82	0.091	0.031	32.7
85703	F2 IV	17 30 49.61	–23 50 29.7	2.55	5.52	7.39	10.46	0.96	0.083	0.037	107.3
85783	B9 II/III	17 31 44.38	–26 16 10.8	0.62	4.02	6.05	7.47	1.10	0.020	0.039	123.1
85797	G2/3 V	17 31 52.07	–31 30 53.8	356.23	1.13	9.55	9.34	1.63	0.037	0.038	54.2
85877	F3 V	17 33 00.37	–24 19 22.5	2.41	4.84	8.48	9.70	1.37	0.065	0.032	169.1
85882	G5 V	17 33 04.02	–25 02 51.3	1.81	4.43	9.66	13.47	1.50	0.042	0.029	138.3
85909	G2/3 V	17 33 20.66	–27 28 10.7	359.80	3.07	9.48	8.62	1.60	0.022	0.025	141.1
85920	G3 V	17 33 29.09	–24 04 17.3	2.69	4.88	8.55	13.91	1.28	0.053	0.018	78.3
85954	F0 IV	17 34 02.39	–23 01 52.6	3.63	5.33	7.36	13.38	2.00	0.033	0.042	179.4
86086	F5 V	17 35 34.06	–24 37 41.3	2.47	4.18	7.70	18.51	1.06	0.053	0.070	168.7
86226	G0 V	17 37 16.09	–24 35 36.1	2.71	3.87	8.72	14.37	1.26	0.073	0.016	54.5
86278	F3 V	17 37 46.85	–23 23 21.4	3.79	4.42	8.28	8.98	1.78	0.083	0.033	140.1
86327	K5	17 38 19.92	–27 12 18.2	0.62	2.28	10.35	18.49	2.22	0.029	0.050	114.8
86376	F5 V	17 39 00.71	–28 24 44.6	359.68	1.51	7.68	12.29	1.07	0.025	0.029	42.8
86385	F8 V	17 39 05.97	–26 56 14.6	0.94	2.28	7.70	19.38	1.18	0.065	0.042	69.5
86633	F0 V	17 42 05.29	–26 50 44.1	1.37	1.76	8.10	5.67	1.08	0.444	0.029	147.1
86719	F8	17 43 08.13	–26 10 37.1	2.06	1.91	10.01	10.16	1.80	0.109	0.051	178.4
86858	F5 V	17 44 48.70	–26 35 19.8	1.91	1.38	8.80	10.21	1.55	0.087	0.010	125.7
86866	G8 IV/V	17 44 54.53	–24 41 02.4	3.55	2.35	8.84	8.77	1.44	0.273	0.024	147.2

Note: Columns 1 to 9 give the HIP number, spectral type, the right ascension and declination for the equinox 2000.0, Galactic longitude and latitude, visual magnitude, trigonometric parallax, and standard error, respectively. Columns 10 and 11 give the obtained linear polarization and measured error, respectively, and Col. 12 the position angle (measured from north to east) of the polarization vector.

Table 2. Measured polarization for some stars contained in the same CCD frames as of the *Hipparcos* stars. For an explanation of each column, see note below.

Star identification	α_{2000} (h m s)	δ_{2000} (° ′ ″)	l (°)	b (°)	P (%)	σ_P (%)	θ (°)
		Field of HIP 83194					
	16 59 48.97	–27 54 38.4	355.16	8.90	0.439	0.116	19.5
	16 59 58.30	–27 54 26.4	355.18	8.87	0.717	0.156	26.9
HD 153351	17 00 07.66	–27 57 11.5	355.17	8.81	0.289	0.062	157.9
GSC 06818−02124	17 00 23.26	–27 59 47.8	355.17	8.74	0.710	0.057	12.6
		Field of HIP 84144					
CD−26 11983	17 11 47.58	–27 05 39.0	357.41	7.24	1.105	0.051	29.2
CD−26 11991	17 12 12.25	–26 58 48.9	357.56	7.23	2.090	0.117	18.3
		Field of HIP 84611					
HD 156198	17 17 29.04	–30 42 58.8	355.17	4.13	0.593	0.012	6.4
		Field of HIP 84888					
HD 156882	17 21 05.61	–27 25 04.5	358.34	5.36	0.091	0.048	90.7
		Field of HIP 85797					
HD 158598	17 31 34.96	–31 29 33.6	356.22	1.20	0.959	0.038	156.7
		Field of HIP 86226					
HD 159746	17 37 19.89	–24 33 54.0	2.74	3.88	0.793	0.053	136.3
		Field of HIP 86327					
	17 38 06.62	–27 15 55.3	0.55	2.29	3.021	0.027	170.3
HD 316049	17 38 28.71	–27 13 00.7	0.63	2.24	3.736	0.108	169.0

Note: Star identification, when available, right ascension and declination for the equinox 2000.0, Galactic longitude and latitude are given in Cols. 1 to 5, respectively. The other columns give the measured linear polarization, measured error, and position angle (measured from north to east) of the polarization vector, respectively.